Stochastic transport of particles in straining flows

D. C. Swailes,* Y. Ammar, and M. W. Reeks
School of Mechanical & Systems Engineering, Newcastle University, Newcastle upon Tyne NE1 7RU, United Kingdom

Y. Drossinos
European Commission, Joint Research Centre, I-21027 Ispra (Va), Italy
(Received 1 November 2008; published 18 March 2009)

Important features associated with the segregration of particles in turbulent flow are investigated by considering the statistical distribution (phase-space number density) of particles subject to the combined effects of straining flow and stochastic forcing. A Fokker-Planck model is used to obtain results for the phase-space distributions of particles that are entrained into straining flow fields. The analysis shows that, in marked contrast to the zero strain case, nonsingular steady-state distributions are generated, and also confirms that the diffusional effect resulting from stochastic forcing is sufficient to offset the otherwise singular distributions that would result from the indefinite accumulation of particles along stagnation lines. The influence of particle inertia (Stokes number) on the form of the resulting distributions is considered and several significant results are observed. The influence of strain rate on the attenuation of particle kinetic stresses is quantified and explained. The development of large third-order velocity moments is observed for Stokes numbers above a critical value. The mechanism underlying this phenomenon is seen to be a generic feature of particle transport in flows where vortex structures induce local counterflows of particles. The system therefore provides an ideal test for closure models for third-order moments of particle velocities, and here the standard Chapman-Enskog approximation is assessed.

DOI: 10.1103/PhysRevE.79.036305 PACS number(s): 47.55.Kf, 05.40.Jc, 82.70.−y, 05.10.Gg

I. INTRODUCTION

Vortex structures in turbulent flow play a dominant role in the distribution and dispersal of aerosols. One important transport mechanism associated with such structures is that in which particulates are ejected from these regions of high vorticity and are focussed within the intervortex regions of high straining (Wang and Maxey [1], Bec [2,3]). The implications of such effects on the formulation of Eulerian models for particle transport are significant, and there have been several recent works concerned with quantifying and developing a deeper understanding of the interaction between the processes involved. These include determination of fractal dimensions characterizing the structures developed within the particle phase (Bec [2,3]), and the description of particle velocity fields in terms of mesoscopic-Eulerian and quasi-Brownian components that account for the decorrelations observed in particle pair velocity structure functions (Février *et al.* [4], Reeks *et al.* [5]). In addition to such phenomena it is also clear that the preferential accumulation of particles in regions of high strain rate will influence rates of agglomeration or coalescence, and that these effects may be further compounded by a secondary transport mechanism induced by fluctuations in the particle motion. These fluctuations originate either from thermal effects (Brownian motion) or the underlying turbulence. In order to build physically realistic models that capture, at some level, the influence of these processes it is necessary to identify and quantify relevant features, and it is the crucial interaction between the effects of straining flow and fluctuating forcing on inertial (nonzero Stokes number St) particles that is the subject of the work presented here.

A key aspect of the models considered here is the white-in-time nature of the stochastic forcing that induces the fluctuations in particle motion, and we envisage two distinct regimes in which this form of forcing is applicable: The first, and most obvious, is the Brownian regime. Typically, this is characterized by $\mathrm{St} \ll 1$, although it is worth noting that even for $\mathrm{St} \sim 1$ the effects of thermally induced Brownian motion may still be relevant at sufficiently high temperatures. One important application in which this could be the case concerns the release of aerosols or particulates from steam generators in nuclear reactor circuits; here the very high flow temperatures mean that, even for relatively large particles, the effects of Brownian diffusion can be significant and may play a crucial role in deposition processes. The second regime concerns relatively high-inertia particles in turbulent flows when, typically, the effective Lagrangian time scale for turbulent velocity fluctuations experienced by a particle is small, and hence $\mathrm{St} \geqslant 1$; in addition, even for these Stokes numbers, particle displacements induced by turbulent velocity fluctuations may still be non-negligible.

Both regimes are studied here, within this common white-in-time framework, via the analysis of a suitably nondimensionalized Fokker-Planck–type transport equation. In addition to the Stokes number St, another nondimensional parameter R appears in this equation. This second parameter, which is distinct from the usual Peclet number Pe, relates characteristic flow to particle velocities and, together with St, determines the relative importance of diffusive to inertial effects.

Estimates of St and R for Brownian motion in a laminar flow (nanoparticle transport in the human respiratory tract) and a turbulent flow (coagulation of water droplets in cumu-

*d.c.swailes@ncl.ac.uk

lus clouds) suggest that diffusive transport is comparable to inertial transport for nanoparticles whose diameter varies from 10 to 100 nm ($\mathrm{St} \sim 10^{-7}-10^{-5}$). Inertial transport dominates (molecular) Brownian transport for $\mathrm{St} \sim 1$. These estimates are only valid for transport in the absence of boundaries, diffusive motion becoming more significant in the boundary layer. Hence, the theoretical analysis presented herein is relevant to coupled inertial and Brownian motion for small Stokes numbers, e.g., nanoparticle transport in microscale geometries. It is, also, relevant to low-Stokes number particle motion in turbulent flow. For example, Chun *et al.* [6] studied the pair radial distribution function of inertial particles for small, but nonzero, Stokes number. They considered their motion in a local linear flow field with a stochastically-varying velocity gradient and acceleration, the corresponding fluctuating forces modelled as Wiener processes. On the other hand, particle diffusion due to turbulent velocity fluctuations is estimated to be comparable to inertial transport for $\mathrm{St} \sim 1$ as we argue in Sec. III. Since the combined effect of straining flow and stochastic forcing on particle dynamics becomes more prominent for large Stokes number we present numerical results for their effect on particle dynamics in a turbulent flow with $\mathrm{St} \sim 1$.

There have been a number of recent studies concerned with the transport of particles dispersed in fluids that exhibit macroscopic flow and uncorrelated velocity fluctuations [7–18]. Furthermore, the motion of non-Brownian particles in shear flows has also received considerable attention: shear-induced self-diffusion of non-Brownian particles in concentrated suspensions has been measured [19], studied numerically [20], and theoretically [21]. More recently, a transition from reversible to irreversible behavior of non-Brownian particles in an oscillatory shear flow has been reported and numerically simulated [22]. Whereas shear-induced particle migration has been studied by Fokker-Planck techniques [21] similar to those presented herein, the physical phenomena involved are different: molecular or turbulent particle diffusion versus fluid-mediated irreversible interparticle interactions. Hydrodynamic interactions of two spherical particles in a linear flow field, neglecting Brownian motion, were first studied by Batchelor and Green [23].

Primary interest in most of these studies has been the influence of the flow on the statistical measures that characterize the dynamics and spatial distribution of the particle phase. Of particular importance in this regard are the particle velocity correlation tensor and the diffusion tensor in the associated convection-diffusion (Smoluchowski) equation. Allied to this is the underlying issue of how the classical fluctuation dissipation theorem that is invoked when modelling Brownian motion in macroscopically quiescent fluids must be modified to accommodate the influence of the flow. Most studies have considered linear (or linearly approximated) flow fields, with simple shear flows predominating [7–12,18], although pure rotational, pure shear (elongational) and pure straining flows have also received some attention [13–16]. While a range of linear flows have been treated in considerable detail a notable exception is the case of a pure straining (or symmetric shear) flow. Although transport in this type of flow field has been addressed in the past, it has not been studied to the same extent and detail as other linear

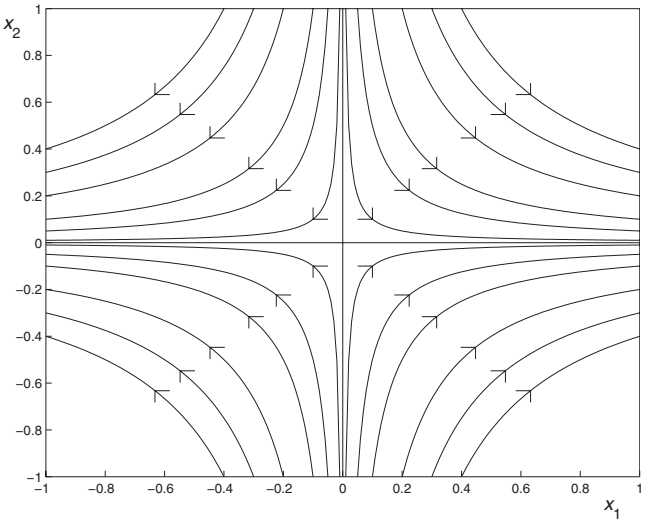

FIG. 1. Streamlines in a 2D pure straining flow.

flows. It is this flow regime that is considered here, and Fig. 1 shows characteristic streamlines.

This fundamental flow can be considered representative of the regions of high strain rate inherent in more complex flows (including coherent structures in turbulent flows), and therefore provides an ideal system by which to study the influence of such flow structures on the behavior of dispersed particles being transported in the flow. Martin and Meiburg [24] considered a model of this form in the context of their work on the dispersion of particles in mixing layers, where they used an array of vortices to model this type of layer. The flow field depicted in Fig. 1 can be interpreted as representing a region at the interface of such vorticial structures which can play a crucial role in particle accumulation.

From a slightly different perspective we can imagine the flow depicted in Fig. 1 as representing the localized straining component of the fluid velocity field as viewed from the frame of reference of a moving particle, centered on $\mathbf{x}=0$ in this coordinate frame. This system can therefore also be used to study the effect straining regions on particle agglomeration, as in the seminal work of Saffman and Turner [25] on droplet collision rates. In this context it is worth noting that, as observed by Fernández de la Mora and Rosner [26], Brownian transport can play a crucial role in agglomeration due to the existence of a Brownian sublayer in the vicinity of a particle surface.

Another motivation for studying this type of flow is that it can be used as a simple model for an impinging jet; the jet corresponding to the flow in the upper half plane and the horizontal axis representing the incident surface. By introducing particles sources symmetrically in the upper and lower half planes we obtain a model in which we can interpret this surface as one at which particles transported in the jet undergo perfectly elastic collisions when impacting the wall (Morrison [27]).

A feature common to many previous studies is that the models considered describe systems in which all the particles are imagined to be injected into the flow at some fixed instant in time. The resulting statistical analysis then provides a description of a transient particle phase generated as the par-

ticles disperse from such an instantaneous source. In most cases this does not lead to the development of a genuine steady-state spatial concentration of particles (other than infinitely dilute). However, in the context of developing Eulerian models and associated closure approximations for particle transport it is often the form of quasisteady, as opposed to transient, features that are of interest. To this end two distinct scenarios are considered here. In Sec. III we consider the case in which particles are injected simultaneously into the flow and allowed to disperse. We analyze the resulting phase-space distribution of such particles. That is, the distribution the particles in terms of their positions and velocities. This analysis not only complements many previous studies but also enables a subsequent analysis for the second scenario, in which we imagine particles being entrained continuously into the flow from distributed, far-field sources. By allowing particles to be continuously injected in this way we can investigate the potential of the system to develop nontrivial steady-state phase-space distributions. Further, we can assess the effect of such continuous sources on the resulting forms of the corresponding particle statistics, and the consequences of these for the construction of constitutive models and closure approximations. This second scenario is examined in Sec. IV, where various fundamental and nontrivial features exhibited by the particle phase-space distributions are established, and the role of Stokes number in the development of these features investigated. Of particular note is the ability of the particle phase to form true, nonsingular steady-state phase-space distributions. As we show, this is made possible only through the subtle interaction between the straining and the forcing. This result is in marked contrast to the zero strain case, where no steady-state is obtained, and also confirms that the diffusional effect resulting from stochastic forcing is sufficient to offset the otherwise singular distributions that would result from the indefinite accumulation of particles along stagnation lines. An analysis of the resulting steady-states highlights several important properties: We show how the straining flow affects the different components of the particle kinetic stresses, serving to attenuate one normal stress component whilst augmenting the other. Further, despite the imposed, uncorrelated Gaussian nature of the underlying forcing, nonzero particle shear-stresses and large third-order moments of the particle fluctuating velocity can develop for Stokes numbers above a critical value. The physical mechanisms behind these effects are explained, and the implication of such features on the formulation and application of appropriate constitutive models and moment closure approximations is illustrated by reference to the standard Chapman-Enskog approximation.

II. BASIC MODEL

A steady, incompressible, two-dimensional, pure straining flow, as depicted in Fig. 1, is defined by a velocity field $\mathbf{u}=(u_1,u_2)$ of the form

$$\mathbf{u}=(\gamma x_1,-\gamma x_2), \tag{1}$$

where γ defines the strain rate of the flow. Attention is confined to the study of noninteracting particles transported in such flows, with trajectories $\mathbf{x}_p(t)$ governed by a stochastic equation of motion of the form

$$\ddot{\mathbf{x}}_p=\dot{\mathbf{v}}_p=\beta[\mathbf{u}(\mathbf{x}_p)-\mathbf{v}_p]+\mathbf{f}, \tag{2}$$

where, consistent with the Stokes drag term in Eq. (2), the particle response rate is modeled as

$$\beta=\frac{6\pi\eta a}{m}, \tag{3}$$

η denotes the fluid viscosity, a the particle radius, and m the particle mass. Fluctuations in particle acceleration due to stochastic forcing are modeled in Eq. (2) via $\mathbf{f}(t)$, which is taken to be a zero-mean, delta-correlated Gaussian process with

$$\langle\mathbf{f}(s)\mathbf{f}(t)\rangle=q^2\delta(s-t)I. \tag{4}$$

The value of parameter q, which defines the intensity of the fluctuating accelerations, is linked to fluid and particle properties and will depend on the nature of the system being considered. In the case of thermally induced Brownian motion (as opposed to that originating from turbulent velocity fluctuations) the simplest and most widely used model, based on the classic fluctuation dissipation theorem, is given by

$$\frac{1}{2}q^2=\frac{\beta kT}{m}. \tag{5}$$

Here k denotes Boltzmann's constant and T the absolute temperature. This model for q (more precisely, the model for the correlations $\langle\mathbf{ff}\rangle$) is based on equilibrium considerations in a quiescent fluid ($\gamma=0$). Several previous works (Santamaría-Holek *et al.* [9], Miyazaki and Bedeaux [10]) have considered the validity of this model in the context of fluids exhibiting macroscopic flow. However, as noted by Drossinos and Reeks [7], provided the time scale of the Brownian driving force is much shorter than that for the imposed flow the effect of the flow on the Brownian correlations can be neglected. Therefore, when considering Brownian motion, we shall adopt the model given by Eq. (5).

The second regime that we can consider to be modeled by Eqs. (2) and (4) is that in which the stochastic motion of the particles is induced by turbulent fluctuations $\mathbf{u}'$ of the fluid velocity field. So that $\mathbf{u}$ is then to be interpreted as a mean velocity field for the fluid. This model can be considered appropriate for high-inertia particles, where a suitably defined Lagrangian time scale τ for turbulent velocity correlations along particle trajectories is small compared to the intrinsic particle response time β^{-1}. In this regime, following Swailes and Reeks [28], we then have

$$\frac{1}{2}q^2=\frac{\beta^2\tau u^2}{1+\beta\tau}, \tag{6}$$

where u^2 represents a characteristic local mean-square fluctuating fluid velocity. Equations (5) and (6) define corresponding mean-square fluctuation particle velocities

$$V^2 = \frac{q^2}{2\beta} = \begin{cases} \dfrac{kT}{m} & \text{Brownian fluctuations,} \\ \dfrac{\beta\tau}{1+\beta\tau}u^2 & \text{turbulent fluctuations.} \end{cases} \tag{7}$$

Typically, in the case of turbulent flow, we have $\gamma\tau \sim 1$. This prompts the definition of particle Stokes number $\mathrm{St} = \gamma/\beta$. As indicated in the introduction the thermally induced Brownian motion regime is then normally characterized by $\mathrm{St} \ll 1$ while, for the turbulent flow interpretation, we should consider $\mathrm{St} \geqslant 1$. In either case, the contribution of diffusive and inertial effects to particle dynamics can be considered by suitable interpretation of q (or V^2) in Eq. (7).

The components of the equation of motion defined by Eqs. (1) and (2) are decoupled and can be written

$$\ddot{x}_j + \beta\dot{x}_j \pm \beta\gamma x_j = q\Gamma \tag{8}$$

with $\Gamma(t)$ the standard, zero-mean, delta-correlated Gaussian process. Here and throughout we interpret $\pm$ as $+$ when $j=1$ and $-$ when $j=2$. This decoupling and similarity in form simplifies the analysis. Note that the x_2 component of particle motion can be interpreted in terms of a harmonic oscillator that will be underdamped if $\beta < 4\gamma$ $(\mathrm{St} > \frac{1}{4})$, in which case the mean particle trajectories will oscillate about $x_2 = 0$. If $\mathrm{St} = \frac{1}{4}$ then the system will be critically damped, while if $\mathrm{St} < \frac{1}{4}$ it will be overdamped.

Our interest is in transient and asymptotic features of the disperse phase generated when particles governed by Eq. (2) are released into the flow. We begin by reviewing the case where this release takes the form of an instantaneous point source of particles. This then provides the foundation for studying other more complex scenarios involving continuous sources.

III. INSTANTANEOUS PARTICLE SOURCE

In order to investigate and emphasize the influence of St on particle dynamics it is convenient to introduce suitably scaled, nondimensional variables. Specifically we take the scalings $t \mapsto \gamma^{-1}t$, $\mathbf{x} \mapsto l\mathbf{x}$ and $\mathbf{v} \mapsto U\mathbf{v}$ where $U = \gamma l$ represents the magnitude of a characteristic local fluid velocity. Then the PDF $p(\mathbf{x}, \mathbf{v}, t | \mathbf{x}^0, \mathbf{v}^0, t^0)$, defining the joint distribution (in terms of these scaled variables) of the particle position $\mathbf{x}$ and velocity $\mathbf{v}$ at time t given that $\mathbf{x}_p = \mathbf{x}^0$ and velocity $\mathbf{v}_p = \mathbf{v}^0$ at time $t^0 < t$, satisfies the Fokker-Planck equation

$$\mathrm{St}\left(\frac{\partial}{\partial t}p + \frac{\partial}{\partial \mathbf{x}} \cdot \mathbf{v}p\right) + \frac{\partial}{\partial \mathbf{v}} \cdot (\Delta \cdot \mathbf{x} - \mathbf{v})p = \frac{1}{R}\frac{\partial^2}{\partial \mathbf{v}^2}p \tag{9}$$

with initial $(t = t^0)$ condition $p = \delta(\mathbf{x} - \mathbf{x}^0)\delta(\mathbf{v} - \mathbf{v}^0)$. In Eq. (9) $\Delta = \mathrm{diag}(1, -1)$ and $R = U^2/V^2 = 2/(q^2\mathrm{St})$, with V^2 defined by one or other of the formulae in Eq. (7), depending on context, and with the nondimensional measure of the fluctuating accelerations $q^2 \mapsto q^2/(\gamma U^2)$.

It is the analysis of the model given by Eq. (9) that allows us to identify the relative contributions of inertial and diffusive effects (as characterized by St and R) to the distribution and transport of particles. The solution to this equation is well-known and leads to the following general expressions for the particle density ρ, mean velocity field $\bar{\mathbf{v}}$, and kinetic stresses $\overline{\mathbf{cc}}$ $(\mathbf{c} = \mathbf{v} - \bar{\mathbf{v}})$ (Swailes and Darbyshire [29])

$$\rho = \frac{1}{2\pi}\det[\Theta_{11}]^{-1/2}\exp\left[-\frac{1}{2}(\mathbf{x} - \hat{\mathbf{x}}) \cdot \Theta_{11}^{-1} \cdot (\mathbf{x} - \hat{\mathbf{x}})\right],$$

$$\bar{\mathbf{v}} = \hat{\mathbf{v}} + \Theta_{21} \cdot \Theta_{11}^{-1} \cdot (\mathbf{x} - \hat{\mathbf{x}}),$$

$$\overline{\mathbf{cc}} = \Theta_{22} - \Theta_{21} \cdot \Theta_{11}^{-1} \cdot \Theta_{12}. \tag{10}$$

In the above expressions $\hat{\mathbf{x}} = \langle \mathbf{x}_p \rangle$, $\hat{\mathbf{v}} = \langle \mathbf{v}_p \rangle$, and the 2×2 matrices Θ_{ij} form the blocks of the particle phase-space covariance matrix $\Theta(t)$. The phase-space mean $\mathbf{m} = (\hat{\mathbf{x}}, \hat{\mathbf{v}})$ and covariance Θ are given by

$$\mathbf{m} = \exp[t\mathrm{A}] \cdot \mathbf{m}^0,$$

$$\Theta = \int_0^t \exp[s\mathrm{A}] \cdot \mathrm{B} \cdot \exp[s\mathrm{A}^\top] ds, \tag{11}$$

where $\mathbf{m}^0 = (\mathbf{x}^0, \mathbf{v}^0)$ and

$$\mathrm{A} = \frac{1}{\mathrm{St}}\begin{pmatrix} 0 & \mathrm{St}I \\ \Delta & -I \end{pmatrix}, \quad \mathrm{B} = \frac{2}{\mathrm{St}R}\begin{pmatrix} \mathbf{0} & \mathbf{0} \\ \mathbf{0} & I \end{pmatrix}. \tag{12}$$

For noncritically damped systems $(\mathrm{St} \neq \frac{1}{4})$ Eq. (11) leads to the following well-established expressions for the components $\hat{x}_j$, $\hat{v}_j$, of $\mathbf{m}$ and the components $\vartheta_{mn}^{(j)}$ of the covariance matrix Θ (Risken [30]):

$$\hat{x}_j = c_1^{(j)}e^{\lambda_1^{(j)}t} + c_2^{(j)}e^{\lambda_2^{(j)}t},$$

$$\hat{v}_j = c_1^{(j)}\lambda_1^{(j)}e^{\lambda_1^{(j)}t} + c_2^{(j)}\lambda_2^{(j)}e^{\lambda_2^{(j)}t}, \tag{13}$$

$$\pm\vartheta_{11}^{(j)} = \frac{1}{Rr_j^2}\left[\lambda_2^{(j)}e^{2\lambda_1^{(j)}t} + \lambda_1^{(j)}e^{2\lambda_2^{(j)}t} \pm 4(1 - e^{-(1/\mathrm{St})t}) + \frac{1}{\mathrm{St}}\right],$$

$$\vartheta_{21}^{(j)} = \vartheta_{12}^{(j)} = \frac{1}{\mathrm{St}Rr_j^2}[e^{2\lambda_1^{(j)}t} + e^{2\lambda_2^{(j)}t} - 2e^{-(1/\mathrm{St})t}],$$

$$\vartheta_{22}^{(j)} = \frac{1}{\mathrm{St}Rr_j^2}\left[\lambda_1^{(j)}e^{2\lambda_1^{(j)}t} + \lambda_2^{(j)}e^{2\lambda_2^{(j)}t} \pm 4(1 - e^{-(1/\mathrm{St})t}) + \frac{1}{\mathrm{St}}\right], \tag{14}$$

with

$$c_1^{(j)} = \frac{1}{r_j}(\lambda_2^{(j)}x_j^0 - v_j^0), \quad \lambda_1^{(j)} = -\frac{1}{2\mathrm{St}}(1 + \sqrt{1 \pm 4\mathrm{St}}),$$

$$c_2^{(j)} = -\frac{1}{r_j}(\lambda_1^{(j)}x_j^0 - v_j^0), \quad \lambda_2^{(j)} = -\frac{1}{2\mathrm{St}}(1 - \sqrt{1 \pm 4\mathrm{St}}), \tag{15}$$

and $r_j = \frac{1}{\mathrm{St}}\sqrt{1 \pm 4\mathrm{St}}$. It should be noted that the eigenvalues $\lambda_1^{(1)}$, $\lambda_2^{(1)}$ associated with motion in the x_1 direction are both real with $\lambda_1^{(1)} < 0$ and $\lambda_2^{(1)} > 0$. In contrast $\lambda_1^{(2)}$, $\lambda_2^{(2)}$, which relate to motion in the x_2 direction, will be complex in the underdamped regime, but in all cases the real parts of both

$\lambda_1^{(2)}$ and $\lambda_2^{(2)}$ will be negative. These properties are central to the large t asymptotic analysis.

The critically damped case is less well documented, but evaluation of Eq. (11) in this case shows that Eqs. (13) and (14), with $j=2$, are replaced by

$$\hat{x}_2 = [(1+2t)\hat{x}_2^0 + t\hat{v}_2^0]e^{-2t},$$

$$\hat{v}_2 = [-4t\hat{x}_2^0 + (1-2t)\hat{v}_2^0]e^{-2t}, \tag{16}$$

$$\vartheta_{11}^{(2)} = +\frac{1}{8R}[2-(1+4t)^2 e^{-4t}],$$

$$\vartheta_{21}^{(2)} = \vartheta_{12}^{(2)} = -\frac{1}{4R}[1-(4t)^2]e^{-4t},$$

$$\vartheta_{22}^{(2)} = +\frac{1}{2R}[2-(1-4t)^2 e^{-4t}]. \tag{17}$$

Using the above expressions a detailed evaluation of the corresponding forms of ρ, $\bar{\mathbf{v}}$, and $\overline{\mathbf{cc}}$ as defined by Eq. (10) is possible. This analysis shows that as $t\to\infty$ the particle density decays exponentially;

$$\rho \sim e^{-\lambda_2^{(1)} t}. \tag{18}$$

As we shall see when we come to consider the potential of the system to generate genuine, nontrivial steady-state distributions, the exponential form of this decay is critical. Further asymptotic analysis shows that the mean particle velocity field and kinetic stresses also approach limiting values. Specifically

$$\bar{\mathbf{v}} \to (\lambda_2^{(1)} x_1, 0) \tag{19}$$

and

$$\overline{c_1 c_1} \to \frac{2}{(1+\sqrt{1+4\mathrm{St}})R}, \quad \overline{c_2 c_2} \to \frac{1}{R}. \tag{20}$$

In view of the uncoupled component equations of motion and the independent components of the stochastic forcing it follows that $\overline{c_1 c_2} \equiv 0$ for all t. Consistent with the fluctuation dissipation theorem, the asymptotic expression for $\overline{c_2 c_2}$ is the standard result for the equilibrium fluctuating energy of a damped harmonic oscillator (Titulaer [31]), and shows that the fluid strain rate does not affect this component of the particle kinetic stresses. However, it is significant that $\overline{c_1 c_1}$ is attenuated by the straining. The physical mechanism for this effect can be understood by considering the corresponding kinetic stress transport equation (Swailes *et al.* [32]):

$$\frac{D}{Dt}\overline{\mathbf{cc}} = -\frac{1}{\rho}\nabla\cdot\overline{\rho\mathbf{ccc}} - \overline{\mathbf{cc}}\cdot\nabla\bar{\mathbf{v}} - \nabla\bar{\mathbf{v}}^{\top}\cdot\overline{\mathbf{cc}} + \frac{2}{St}\left(\frac{1}{R}I - \overline{\mathbf{cc}}\right). \tag{21}$$

The Gaussian form of the phase-space distribution implies that $\overline{\mathbf{ccc}} \equiv 0$. Further, since $\overline{c_1 c_2} \equiv 0$ and (for large time) $\bar{\mathbf{v}} = (\lambda_2^{(1)} x_1, 0)$, it follows from Eq. (21) that the asymptotic form of $\overline{\mathbf{cc}}$ satisfies

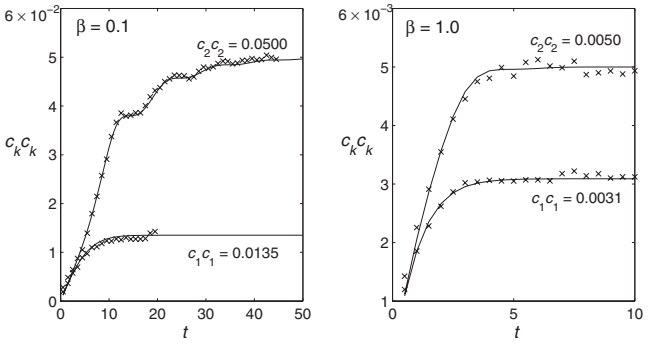

FIG. 2. Components $\overline{c_k c_k}(t)$.

$$-\overline{\mathbf{cc}}\cdot\frac{1}{2}(\nabla\bar{\mathbf{v}} + \nabla\bar{\mathbf{v}}^{\top}) + \frac{1}{\mathrm{St}}\left(\frac{1}{R}I - \overline{\mathbf{cc}}\right) = 0. \tag{22}$$

Rearranging Eq. (22) for $\overline{\mathbf{cc}}$ leads directly to the results given by Eq. (20). From Eq. (22) we see that the attenuation in $\overline{c_1 c_1}$ is attributable to the dissipation of the fluctuating kinetic energy due to work done by the kinetic stresses. This dissipation decreases with St. We also observe that, as in the case of a simple shear (Drossinos and Reeks [7]), the particle phase, considered as a continuum, cannot be treated in terms of a Newtonian flow, since the particle pressure tensor $\rho\overline{\mathbf{cc}}$ is not linearly proportional to $\nabla\bar{\mathbf{v}}+\nabla\bar{\mathbf{v}}^{\top}$. By way of validating the above results Fig. 2 shows the time evolution of the two nonzero components of $\overline{\mathbf{cc}}$, as generated by an instantaneous point source and as computed from the analytical solution, together with corresponding simulation results obtained from a simple particle tracking code. The predicted asymptotic values, as defined by Eq. (20), are also indicated in the figure, and these are seen to be reached in the large time limit. To emphasize the attentuation in $\overline{c_1 c_1}$ we have taken $\mathrm{St}\geqslant 1$ and, consequently, have adopted the "turbulence" interpretation of q in Eq. (7). Further, taking $u \sim U/10$ as typical for turbulent root-mean-square velocities we have $R\mathrm{St}\sim 200$ and, with $U\sim 1$, this implies $q\sim 0.1$. For this reason, in the results we present we have fixed $q=0.1$ and $R\mathrm{St}=200$.

Allied to Eq. (19) we also find that $\hat{\mathbf{v}}\to\bar{\mathbf{v}}(\hat{\mathbf{x}})$, showing that $\langle\mathbf{v}_p\rangle$ does not asymptotically approach $\langle\mathbf{u}(\mathbf{x}_p)\rangle$ as $t\to\infty$. This has implications for the construction of convection-diffusion models for particle transport in this type of system: Using the particle-phase continuity equation

$$\frac{\partial}{\partial t}\rho + \frac{\partial}{\partial\mathbf{x}}\cdot\rho\bar{\mathbf{v}} = 0 \tag{23}$$

together with Eq. (10) we obtain the following generalized Smoluchowski equation for the particle concentration ρ:

$$\frac{\partial}{\partial t}\rho + \frac{\partial}{\partial\mathbf{x}}\cdot\rho(\mathbf{u}+\hat{\mathbf{v}}-\Delta\cdot\hat{\mathbf{x}}) = \frac{\partial}{\partial\mathbf{x}}\cdot D\cdot\frac{\partial}{\partial\mathbf{x}}\rho, \tag{24}$$

where the nondimensionalized time-dependent diffusion tensor D is given by

$$D(t) = \langle(\mathbf{v}^*-\mathbf{u}^*)\mathbf{x}^*\rangle = \Theta_{21} - \Delta\Theta_{11}. \tag{25}$$

Here $\mathbf{x}^*=\mathbf{x}_p-\hat{\mathbf{x}}$, $\mathbf{v}^*=\mathbf{v}_p-\hat{\mathbf{v}}$, and $\mathbf{u}^*=\mathbf{u}(\mathbf{x}^*)$. Equations (24) and (25) are valid for any linear flow $\mathbf{u}=\boldsymbol{\alpha}\cdot\mathbf{x}$, (replacing Δ

with $\boldsymbol{\alpha}$). Since, in the flow considered here, $\hat{\mathbf{v}}$ does not converge to $\mathbf{u}(\hat{\mathbf{x}})$ in the large time limit, we see that this contribution to the convective term on the left-hand side of Eq. (24) cannot be neglected. This is in contrast to the simple shear (Drossinos and Reeks [7]). The decoupling of the component equations of motion Eq. (8) means that the diffusion tensor D also has a diagonal form $D=\mathrm{diag}(d_1,d_2)$ and, using Eq. (14),

$$d_j = \frac{\mathrm{St}}{(1 \pm 4\mathrm{St})R}[(1+\lambda_2^{(j)}\mathrm{St})e^{2\lambda_1^{(j)}t} + (1+\lambda_1^{(j)}\mathrm{St})e^{2\lambda_2^{(j)}t} - 2(1 \pm 2\mathrm{St})e^{-(1/\mathrm{St})t} + 1 \pm 4\mathrm{St}]. \quad (26)$$

The large time asymptotic forms of these nondimensional diffusion coefficients are

$$d_1 \sim \frac{\mathrm{St}(1-\sqrt{1+4\mathrm{St}})}{2R(1+4\mathrm{St})}e^{2\lambda_2^{(1)}t}, \quad d_2 = \frac{\mathrm{St}}{R}. \quad (27)$$

Invoking Eq. (20) we see that, asymptotically, $d_2 \to \mathrm{St}\overline{c_2 c_2}$ or, converting back to unscaled variables, $q^2/2\beta^2$. This agrees with the familiar Stokes-Einstein diffusion coefficient expression. In contrast, the asymptotic value of the diffusion coefficient d_1 is seen to be negative. This is analogous to the case of a simple shear (Drossinos and Reeks [7], Reeks [16]). However, for a simple shear the corresponding diffusion coefficient obtains a finite asymptotic value which is only negative for $\mathrm{St} > \sqrt{2/3}$. Here, in contrast, d_1 is always negative and increases in magnitude without bound. This reflects the focussing of the particles along the x_1 axis and the reference frame centered on $\hat{\mathbf{x}}$, $\hat{\mathbf{v}}$. At first sight this result seems at variance with the expected behavior for small St—when we anticipate $d_1 \sim d_2 \to \mathrm{St}/R$ so that Eq. (24) reduces to the classical Smoluchowski equation appropriate for Brownian motion. The paradox is resolved by noting that, from Eq. (15), $\lambda_1^{(j)} \sim -1/\mathrm{St}$, $\lambda_2^{(j)} \sim \pm 1$ as $\mathrm{St} \to 0$. Consequently, in this regime, we should write

$$d_j \sim \frac{\mathrm{St}}{(1 \pm 4\mathrm{St})R}[(1 \pm \mathrm{St})e^{-(2/\mathrm{St})t} - 2(1 \pm 2\mathrm{St})e^{-(1/\mathrm{St})t} + (1 \pm 4\mathrm{St})] + O(\mathrm{St}^2). \quad (28)$$

From this it follows that for $\mathrm{St} \ll 1$ we obtain, as expected, $d_j \to \mathrm{St}/R$ as $t \to \infty$. There are several important points to note in connection with the results given by Eqs. (27) and (28). First, the classical Smoluchowski equation, with a single scalar (Stokes-Einstein) diffusion coefficient is recovered here for $\mathrm{St} \ll 1$ irrespective of the value of R. However, this is not generally true since gradient diffusion usually requires, in addition, that $R \ll 1$ as a scaling analysis of the momentum equation shows [33]. The reason why the value of R does not play a role here is that the underlying flow field is exactly linear and, consequently, the momentum transport equation necessarily takes a gradient diffusion form when considered in the frame moving with the mean particle coordinates, see Eq. (24), albeit with asymmetric diffusion coefficients. Further, since we can identify a single scalar diffusion coefficient when $\mathrm{St} \ll 1$, it is appropriate in this regime to characterize the relative influence of inertia to diffusion via the corresponding Peclet number. Specifically, in view of the above result for $\mathrm{St} \ll 1$ we can define $\mathrm{Pe}=R/\mathrm{St}$. However, when $\mathrm{St} \geqslant 1$ we see that it is inappropriate to introduce Pe, since the system is no longer characterized by a single meaningful diffusion coefficient, but must consider St and R independently. Having established these results for the case of particles released into the flow at some fix time, we now turn our attention to the situation in which particles are released continuously.

IV. CONTINUOUS PARTICLE SOURCES

The situation in which particles are introduced continuously (at a fixed rate and with a fixed velocity $\mathbf{v}^0$) from spatially distributed sources, models a system in which we imagine particles being entrained into the localized straining flow structure from a far-field reservoir of uniformly distributed particles. In particular we will consider line sources $|x_1| < X_1$, $x_2 = \pm X_2$. By taking sources along both $x_2 = +X_2$ and $x_2 = -X_2$ we preserve the symmetry depicted in Fig. 1. It is important to note that in the absence of stochastic forcing (i.e., with $q=0$) all particle trajectories will converge asymptotically to the x_1 axis; there will be a continual accumulation of particles along this stagnation line and no steady-state will be set up. Similarly, as we shall show, the continuous release of particles into a fluid with zero mean velocity ($\gamma=0$) does not lead to true steady-state distributions. A natural question therefore arises in the context of this system: Do the combined effects of stochastic forcing and straining generate a steady-state distribution of particles and, if so, how do the statistical properties of this distribution differ from those generated by the instantaneous sources considered in Sec. III? To answer these questions we note that the PDF $p(\mathbf{x},\mathbf{v},t)$ describing the phase-space distribution of such particles can be constructed in terms of the PDF's $p(\mathbf{x},\mathbf{v},t|\mathbf{x}^0,\mathbf{v}^0,t_0)$ studied in the previous section: Since γ and $\mathbf{u}$ are constant (in time), and Γ is statistically stationary and homogeneous in time, we can write

$$p(\mathbf{x},\mathbf{v},t) = \int_{\mathbf{x}^0} \phi \int_0^t p(\mathbf{x},\mathbf{v},s|\mathbf{x}^0,\mathbf{v}^0,0)ds d\mathbf{x}^0, \quad (29)$$

where $\phi = \phi(\mathbf{x}^0)$ gives the spatial distribution of the points $\mathbf{x}^0$ from which the particles are released. For the line sources described above

$$\phi(\mathbf{x}^0) = \frac{1}{2X_1}\delta(x_2^0 \pm X_2), \quad |x_1^0| < X_1. \quad (30)$$

With no loss of generality we have taken the constant rate of particle release at each point $\mathbf{x}^0$ to be unity, and have omitted explicit indication of the dependence of p on $\mathbf{v}^0$. From Eq. (29) it follows that the particle statistics generated by a continuous, distributed source can be related in a similar fashion to the corresponding statistics for the instantaneous point source. Specifically

$$\rho = \int_{\mathbf{x}^0} \phi \int_0^t \rho(\mathbf{x},s|\mathbf{x}^0,0)ds d\mathbf{x}^0,$$

$$\rho\bar{\mathbf{v}} = \int_{\mathbf{x}^0} \phi \int_0^t \rho(\mathbf{x},s|\mathbf{x}^0,0)\bar{\mathbf{v}}(\mathbf{x},s|\mathbf{x}^0,0)ds\mathbf{dx}^0, \tag{31}$$

with similar expressions for $\rho\overline{\mathbf{vv}}$ and $\rho\overline{\mathbf{vvv}}$, etc. (Again we omit indication of $\mathbf{v}^0$ dependence from the notation.) Evaluation of these statistics is feasible since, from Eq. (10), we have closed form expressions for the integrands appearing in the right-hand sides of Eq. (31). We are particularly interested in the asymptotic ($t\to\infty$) behavior of the statistics defined by Eq. (31). Crucial to form of this asymptotic behavior is the corresponding behavior of the integrands in Eq. (31), and these have already been discussed in the previous section.

The asymptotic form of the density $\rho(\mathbf{x},t)$ defined by Eq. (31) is determined by the limiting form of

$$\rho(\mathbf{x},t|\mathbf{x}^0) = \int_0^t \rho(\mathbf{x},s|\mathbf{x}^0,0)ds, \tag{32}$$

as $t\to\infty$. The density defined by Eq. (32) represents that generated by a continuous point source—where particles are released continuously, and at a constant rate, from the fixed point $\mathbf{x}^0$. In the same way the asymptotic forms of the particle mean velocity, kinetic stresses, and third-order moments are determined by time histories of corresponding statistics generated from continuous point sources. Some features of these asymptotic forms can be inferred from the underlying transient behavior of the instantaneous point source statistics forming the integrands in Eq. (31). In the previous section we noted that the density $\rho(\mathbf{x},t|\mathbf{x}^0,0)$ generated by an instantaneous point source decays exponentially at each point as $t\to\infty$. Of course we would expect the density generated by an instantaneous point source into an unbounded shear flow to decay to zero. However the exponential form of this decay is crucial, since it ensures that the density, given by Eq. (32), approaches a steady-state value in this limit. This is in contrast to the singular case $\gamma=0$ (no mean flow): In this case it is easy to show, using the corresponding form of Θ_{11}, that $\rho\sim t^{-1}$. This means that the density generated from a continuous source in a statistically stationary fluid increases as $\ln(t)$ for large t, and hence does not reach a true steady-state—only a self-similar form. The instantaneous point source density can be written as $\rho=\rho_1\times\rho_2$ where

$$\rho_1 = \int_{x_2} \rho dx_2, \quad \rho_2 = \int_{x_1} \rho dx_1, \tag{33}$$

are the marginal distributions of ρ, and represent the distributions associated with the component equations of motion Eq. (8). Further, detailed analysis shows that, for large t,

$$\rho_1 \sim e^{-\lambda_2^{(1)}t}, \quad \rho_2 \sim \frac{1}{\sqrt{2\pi}\sigma}\exp\left[-\frac{x_2^2}{2\sigma^2}\right], \tag{34}$$

with

$$\sigma^2 = \frac{\mathrm{St}}{R}. \tag{35}$$

From these asymptotic forms we deduce that the corresponding component density ρ_1 from a continuous point source will reach a steady-state form, whereas ρ_2 will be unbounded, but will approach the self-similar form in Eq. (34) as $t\to\infty$.

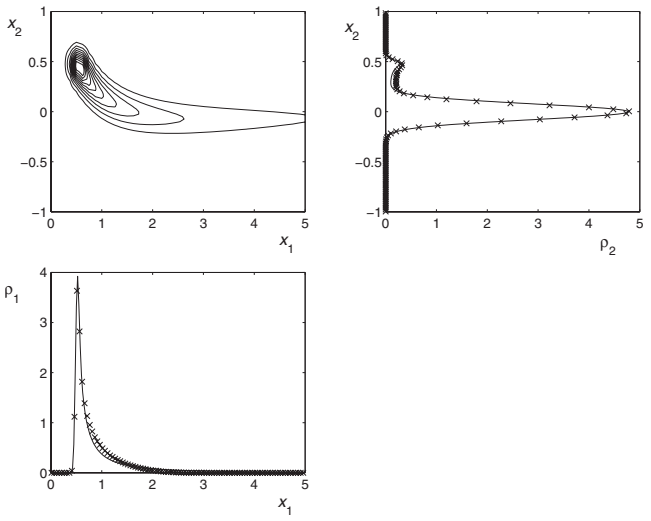

FIG. 3. Particle concentration; CPS, St=1, R=200.

Figure 3 shows the steady-state particle density generated by a continuous point source (CPS) of particles at $\mathbf{x}^0=(0.5,0.5)$. The density contours, derived from the pdf solution, show how the distribution of particles is influenced by the underlying flow.

In Fig. 3 the particle trajectories are underdamped (St=1) and therefore (in the absence of stochastic fluctuations) exhibit periodic oscillations about the x_1 axis. This is reflected in the figure, which indicates that there is a significant concentration of particles in the region $x_2<0$, in accordance with Eq. (35) which shows how the width of the distribution increases with St. Following the discussion in the previous section we note that, for $\mathrm{St}\ll 1$, we can write $\sigma^2=1/\mathrm{Pe}$. The profiles of the marginal densities, ρ_1 ρ_2, presented in Fig. 3, are validated by reference to the corresponding simulation results ($\times$).

By similar reasoning it follows, using Eqs. (18)–(20), that the mass flux $\rho\bar{\mathbf{v}}$ and the second moments $\rho\overline{\mathbf{vv}}$ generated by a continuous point source also approach finite limiting distributions as $t\to\infty$. It is important to note that there are several features of the steady-state statistics generated by a continuous particle source that are intrinsically different from the corresponding forms for an instantaneous source: An instantaneous source produces a particle mean velocity field that is always linear in $\mathbf{x}$, while the kinetic stresses are spatially independent (and $\overline{c_1c_2}\equiv 0$). By contrast, and as illustrated in Figs. 4 and 5, these features do not necessarily hold for a continuous source. The figures show steady-state particle statistics generated by a continuous release of particles from the centre of the straining $\mathbf{x}=\mathbf{0}$. Figure 4 shows asymptotic profiles of the components, $\bar{v}_1$, $\bar{v}_2$, of the particle mean velocity along various lines of constant x_1 and x_2. The essentially linear dependence of $\bar{v}_1$ on x_1, and the near independence from x_2, is a consequence of the fact that the mean velocity $\bar{v}_1$ in the integrand of Eq. (31) converges to the limiting form given by Eq. (19) exponentially at a rate that is greater than that at which the associated density increases

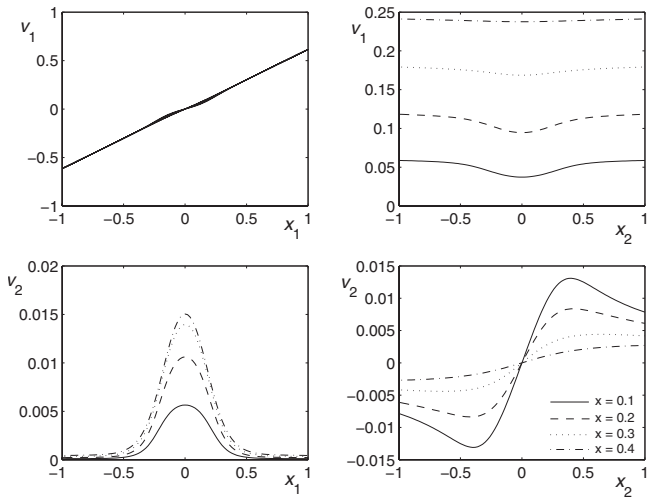

FIG. 4. Mean velocity profiles; CPS $\mathbf{x}^0=\mathbf{0}$, St=1, $R=200$.

from its initial zero value. Therefore the asymptotic mean velocity field $\bar{v}_1$ is essentially the same for both an instantaneous and a continuous point source. The parameter value St=1 used in Fig. 4 give $\lambda_2^{(1)}=\frac{1}{2}(\sqrt{5}-1)=0.618$ in agreement with the graph. We also observe from these graphs the nonlinear spatial variations in $\bar{v}_2$.

Figure 5 depicts contours of the steady-state second-order fluctuating velocity moments $\overline{c_i c_j}$, normalized by reference to the asymptotic values given in Eq. (20). In addition to the fact that these statistics are inhomogeneous, and that c_1c_2 is nonzero, we also note that c_1c_1 actually exceeds the corresponding large time value given by Eq. (20). This somewhat counterintuitive effect is manifest in a more striking way in the results obtained from the line sources $x_2^0=\pm X_2$. Figures 6–9 depict various steady-state particle statistics generated from these types of sources.

The graphs in Fig. 6 show steady-state densities ρ generated from the continuous distributed sources (CDS) defined by Eq. (30) ($X_1=1$, $X_2=1$), with St=0.1, 0.25, 1 (and StR =200). In the underdamped case (St=1) individual particle

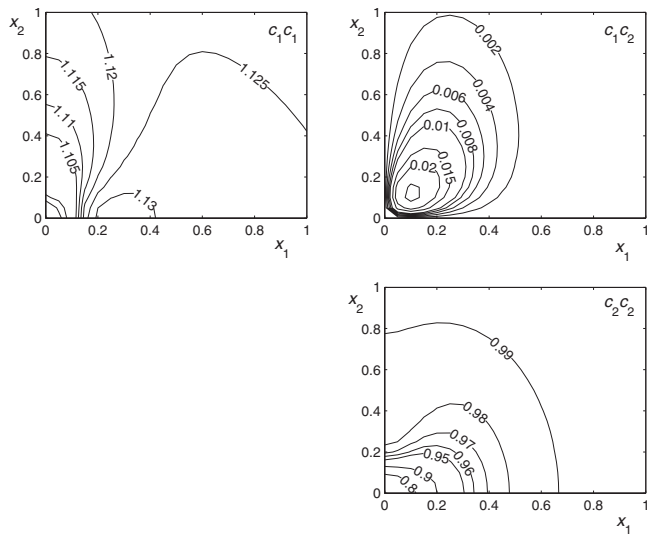

FIG. 5. Normalized $\overline{c_i c_j}$; CPS $\mathbf{x}^0=\mathbf{0}$, St=1, $R=200$.

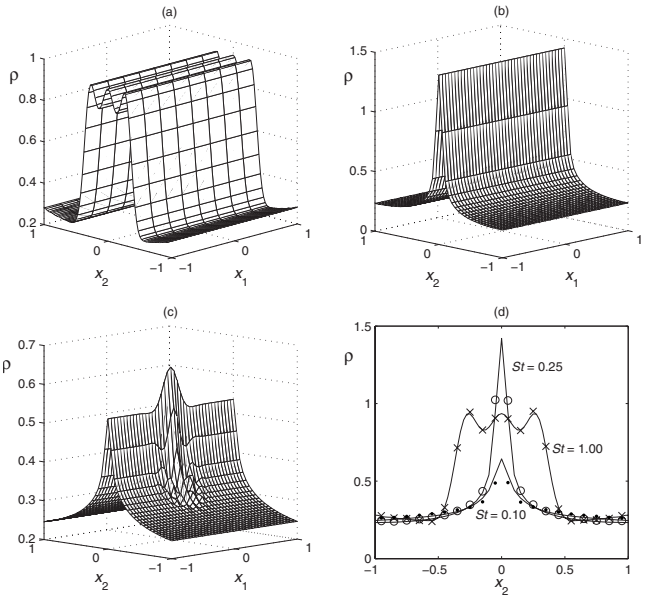

FIG. 6. Spatial distributions; CDS, $R=200/\mathrm{St}$: (a) St=1, (b) St=0.25, (c) St=0.1.

trajectories exhibit damped oscillatory motion in the x_2 component. This is reflected in the trimodal distribution shown in the Fig. 6(a); the central peak, centered on $x_2=0$, is a consequence of the asymptotic form of the particle trajectories focussed along the x_1 axis, while the side peaks are generated by the transient features of the trajectories and are influenced by the turning points in the mean particle motion (where $\langle v_2\rangle=0$). This feature has been noted before; Martin and Meiburg [24] observed bimodal concentration profiles in a system similar to that considered here, but with a single line source and no stochastic forcing.

Clearly we would not expect multimodal concentration profiles to occur for overdamped particles (St<0.25), and this is confirmed by Fig. 6(c), which shows the corresponding distribution for St=0.1. Here, instead, we see that there is

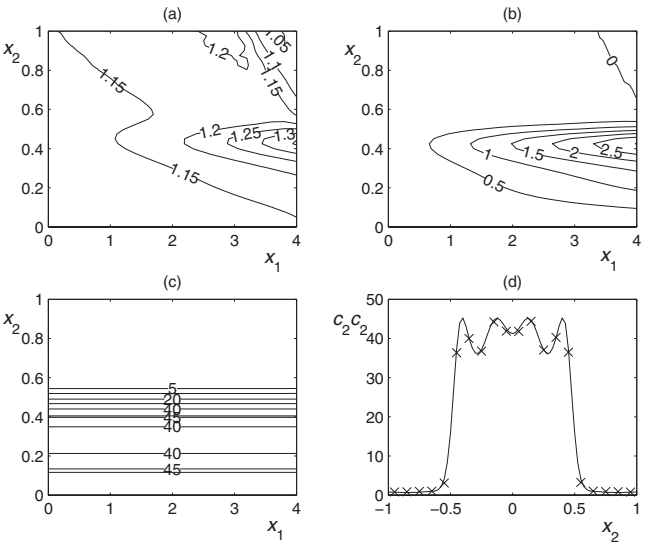

FIG. 7. Normalized $\overline{c_i c_j}$; CDS, St=1, $R=200$: (a) $\overline{c_1c_1}$, (b) $\overline{c_1c_2}$, (c) $\overline{c_2c_2}$.

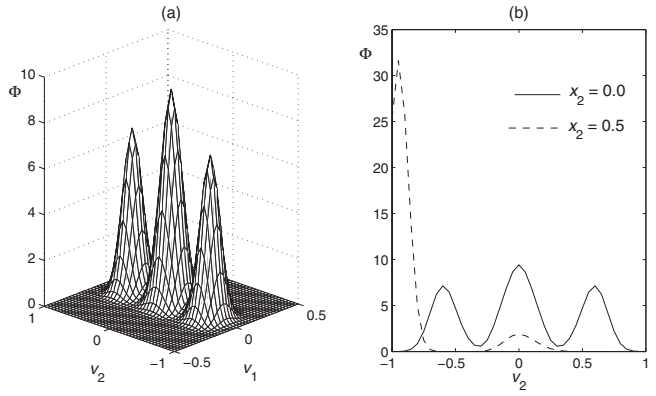

FIG. 8. Velocity distributions; CDS, St=1, R=200: (a) $\Phi(\mathbf{0},\mathbf{v})$, (b) $\Phi(0,x_2,0,v_2)$.

a relatively greater accumulation of particles in the region of the stagnation point $\mathbf{x}=\mathbf{0}$ and, unlike the case St=1, the distribution is not independent of x_1. The critically damped case is shown in Fig. 6(b), and a comparison of the x_2 dependence of these densities along the line $x_1=0$ in Fig. 6(d), which illustrates that the focusing of particles along the x_1 axis is most pronounced at this critical Stokes number. This graph includes data from particle tracking simulations that validate the pdf generated profiles.

Figure 7 shows contours of the steady-state kinetic stresses c_ic_j for the case St=1. Again, these results have been normalized by reference to the large time asymptotic values given in Eq. (20) and, as with Fig. 5, we observe values in excess of these asymptotic statistics. Figure 7(c) is particularly striking in that it shows regions of extremely high values of the normal stress $\overline{c_2c_2}$. Figure 7(d) shows the variation of this stress component with x_2, with simulation data (×) confirming the form of the profile. A physical explanation of the source of this enhanced contribution to the fluctuating kinetic energy comes from consideration of the form of the velocity distribution $\Phi=p/\rho$ obtained for underdamped particle trajectories. Figure 8(a) shows this distribution of velocities at the origin. The trimodal form of this distribution at $\mathbf{x}=\mathbf{0}$ (or more generally along the x_1 axis) is again a consequence of the mean particle trajectories crossing the x_1 axis: Particles from the line source at $x_2=X_2$ contribute to the distribution of predominantly negative v_2 values along the x_1 axis, while the corresponding particles from the source at $x_2=-X_2$ give the peak in the distribution centered on a positive velocity.

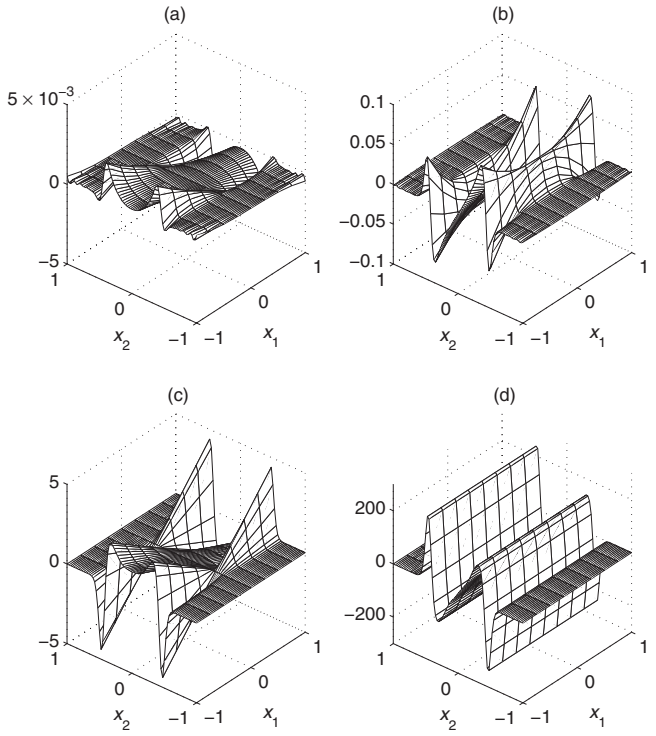

FIG. 9. Normalized $\overline{c_ic_jc_k}$; CDS, St=1, R=200: (a) $\overline{c_1c_1c_1}$, (b) $\overline{c_1c_1c_2}$, (c) $\overline{c_1c_2c_2}$, (d) $\overline{c_2c_2c_2}$.

The interpretation of the stress $\overline{c_2c_2}$ as the variance of the distribution shown in Fig. 8(a) then accounts for the high value of this moment. The symmetry of the velocity distribution shown in Fig. 8(a) is a consequence of the fact that this is observed on the x_1 axis, where both line sources contribute equally. Away from this axis the velocity profiles become asymmetric. This is illustrated in Fig. 8(b) which compares the distribution of v_2 (for $v_1=0$) at $\mathbf{x}=\mathbf{0}$ [as in Fig. 8(a)], with that at $\mathbf{x}=(0.0,0.5)$. At this latter point the line source at $x_2=+X_2$ dominates and so there is a bias in the distribution towards negative values. The second, smaller peak, generated by the other line source, then produces a highly skewed velocity distribution.

A major consequence of this asymmetry is the resulting generation of large third-order moments **ccc** of the fluctuating velocity, a feature that is not normally associated with particles driven by uncorrelated Gaussian forcing. Third-order moments are normally modeled via some form of closure approximation within the framework of mean-field transport equations, e.g., Eq. (21). Our model therefore provides a stringent test case for assessing such closures. To compute these third-order moments we write them in terms of the more directly determined velocity moments $\bar{\mathbf{v}}$, **vv**, and **vvv** which can be computed from the corresponding moments generated by a point source. Figure 9 shows the spatial distribution of the moments $c_ic_jc_k$ for St=1. These moments have been normalized using the asymptotic values given by Eq. (20).

Significant here, and consistent with the results shown in Fig. 8(b), are the high values of $c_2c_2c_2$ which reflect the existence of highly skewed v_2 velocity distributions away from the stagnation line $x_2=0$. As might be expected these moments are less significant for smaller Stokes numbers.

The simplest closure approximation for these third-order moments is the symmetry assumption $\mathbf{ccc}\approx 0$. The results presented here clearly show that this approximation is unlikely to be valid in situations in which particles are being transported in flows exhibiting coherent structures. The alternative closure model that is often invoked is the Chapman-Enskog approximation (Swailes *et al.* [32])

$$\overline{c_ic_jc_k} \approx -\frac{1}{3}\mathrm{St}\left(\overline{c_ic_r}\frac{\partial\overline{c_jc_k}}{\partial x_r}+\overline{c_jc_r}\frac{\partial\overline{c_kc_i}}{\partial x_r}+\overline{c_kc_r}\frac{\partial\overline{c_ic_j}}{\partial x_r}\right). \quad (36)$$

Since $\overline{c_2c_2}$ is essentially independent of x_1 Eq. (36) gives

$$\overline{c_2c_2c_2} \approx -\mathrm{St}\overline{c_2c_2}\frac{\partial \overline{c_2c_2}}{\partial x_2}. \tag{37}$$

To assess this approximation it is therefore necessary to evaluate the third-order stress gradient tensor $\nabla\overline{\mathbf{cc}}$ generated by a continuous source of particles. While these gradients could be estimated numerically this would introduce unnecessary errors into the resulting data, and would also necessitate the computation of $\overline{\mathbf{cc}}$ over a grid of closely spaced points. To avoid this we can again make use of the idea of relating $\nabla\overline{\mathbf{cc}}$ to other gradient terms that can be evaluated directly at any given point. We write

$$\rho\nabla\overline{\mathbf{cc}} = \nabla(\rho\overline{\mathbf{vv}}) - \nabla(\rho\overline{\mathbf{v}}\overline{\mathbf{v}}) - (\nabla\rho)\overline{\mathbf{cc}}, \tag{38}$$

with

$$\nabla(\rho\overline{\mathbf{vv}}) = \int_0^\infty (\nabla\rho)(\overline{\mathbf{v}}\overline{\mathbf{v}} + \overline{\mathbf{cc}}) + \rho[(\nabla\overline{\mathbf{v}})\overline{\mathbf{v}} + \overline{\mathbf{v}}\nabla\overline{\mathbf{v}}]ds, \tag{39}$$

$$\nabla(\rho\overline{\mathbf{v}}\overline{\mathbf{v}}) = \left(\int_0^\infty (\nabla\rho)\overline{\mathbf{v}} + \rho\nabla\overline{\mathbf{v}}ds\right)\overline{\mathbf{v}} + \overline{\mathbf{v}}\left(\int_0^\infty (\nabla\rho)\overline{\mathbf{v}} + \rho\nabla\overline{\mathbf{v}}ds - \int_0^\infty \nabla\rho ds\overline{\mathbf{v}}\right), \tag{40}$$

and

$$(\nabla\rho)\overline{\mathbf{cc}} = \int_0^\infty \nabla\rho ds\overline{\mathbf{cc}}. \tag{41}$$

The gradients in integrands are obtained directly from Eq. (10). Specifically we get

$$\nabla\rho = -\rho\Theta_{11}^{-1}\cdot(\mathbf{x}-\hat{\mathbf{x}}), \tag{42}$$

$$\nabla\overline{\mathbf{v}} = \Theta_{11}^{-1}\cdot\Theta_{12}. \tag{43}$$

These relationships have been used to compute the asymptotic form of $\nabla\overline{\mathbf{cc}}$ generated by continuous line sources, and hence assess the validity of the approximation given by Eq. (37). Figure 10 compares values for the expressions on both sides of Eq. (37) (normalized as before), and again includes simulation results that validate the PDF generated values of $\overline{c_2c_2c_2}$.

The figure shows that this approximation also does not perform well in the present context. Given that the approximation is based on perturbative corrections to Gaussian velocities it is perhaps not surprising that the agreement is so poor, but it does emphasize that even relatively simple Brownian systems can require more sophisticated closures than those that are commonly used.

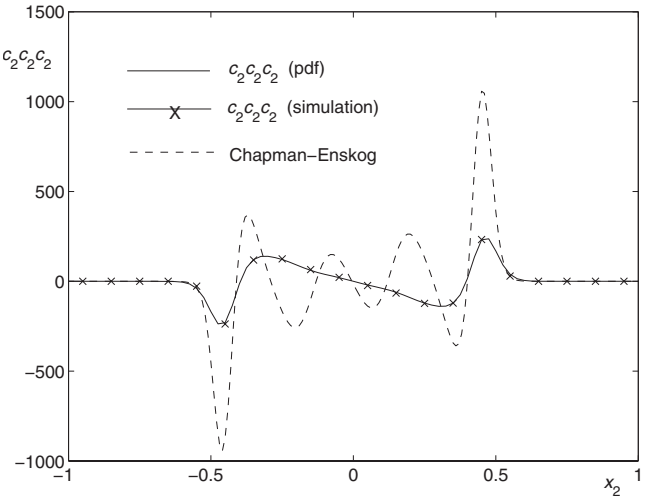

FIG. 10. Chapman-Enskog approximation (37); CDS, St=1, R =200.

V. CONCLUSIONS

Making use of a Fokker-Planck–type model we have analyzed the evolution of statistical properties of particles released, both instantaneously and continuously from distributed sources, into flows exhibiting a symmetrically strained mean velocity field on which stochastic fluctuations are superposed to model the effects of either Brownian or turbulent motion. Several important features of the resulting particle distributions have been observed which have consequences for the modeling of such systems in terms of transport equations for the particle number density, mean velocity, and kinetic stresses. In particular, the role of Stokes number on the attenuation of particle kinetic stresses by the straining flow and the development of large third-order moments of the particle fluctuating velocity have been investigated. Moreover, it is clear that the observed phenomenon of multimodal, highly skewed velocity distributions is not limited to underdamped particles in idealized symmetric straining flows, but is a generic feature of particle transport in turbulent flows in which vortex structures induce local counterflows of particles. The construction of improved closures for third-order velocity moments is therefore of fundamental importance, and the system considered here is seen to offer a simple but critical test of such closure modeling. The construction of such closure approximations is the subject of on-going study.

ACKNOWLEDGMENTS

The authors acknowledge the EPSRC (Grant No. EP/D061601/1) and the Paul Scherrer Institute, Switzerland for their financial support of this work.

[1] L. Wang and M. Maxey, J. Fluid Mech. **256**, 27 (1993).
[2] J. Bec, Phys. Fluids **15**, L81 (2003).
[3] J. Bec, J. Fluid Mech. **528**, 255 (2005).
[4] P. Février, O. Simonin, and K. Squires, J. Fluid Mech. **533**, 1 (2005).
[5] M. Reeks, L. Fabbro, and A. Soldati (unpublished).
[6] J. Chun, D. Koch, S. Rani, A. Ahluwalia, and L. Collins, J. Fluid Mech. **536**, 219 (2005).
[7] Y. Drossinos and M. W. Reeks, Phys. Rev. E **71**, 031113 (2005).
[8] G. Subramanian and J. Brady, Physica A **334**, 343 (2004).
[9] I. Santamaría-Holek, D. Reguera, and J. M. Rubí, Phys. Rev. E **63**, 051106 (2001).
[10] K. Miyazaki and D. Bedeaux, Physica A **217**, 53 (1995).
[11] P. Schram and S. Trigger, Physica B **228**, 91 (1996).
[12] M. Valdez and O. Manero, J. Colloid Interface Sci. **190**, 81 (1997).
[13] R. T. Foister and T. G. M. van de Ven, J. Fluid Mech. **80**, 105 (1980).
[14] R. Mauri and S. Haber, SIAM J. Appl. Math. **46**, 49 (1986).
[15] D. Swailes and K. Darbyshire, Physica A **262**, 307 (1999).
[16] M. Reeks, J. Fluid Mech. **522**, 263 (2005).
[17] H. S. Wio and D. H. Zanette, Phys. Rev. E **47**, 384 (1993).
[18] D. Elrick, Aust. J. Phys. **15**, 283 (1962).
[19] D. Leighton and A. Acrivos, J. Fluid Mech. **177**, 109 (1987).
[20] M. Marchioro and A. Acrivos, J. Fluid Mech. **443**, 101 (2001).
[21] A. Sierou and J. Brady, J. Fluid Mech. **506**, 285 (2004).
[22] D. Pine, J. Gollub, J. Brady, and A. Leshansky, Nature (London) **438**, 997 (2005).
[23] G. Batchelor and J. Green, J. Fluid Mech. **56**, 375 (1972).
[24] J. Martin and E. Meiburg, Phys. Fluids **6**, 1116 (1994).
[25] P. Saffman and J. Turner, J. Fluid Mech. **1**, 16 (1956).
[26] J. Fernández de la Mora and D. Rosner, J. Fluid Mech. **125**, 379 (1982).
[27] F. Morrison, J. Aerosol Sci. **5**, 241 (1974).
[28] D. Swailes and M. Reeks, Phys. Fluids **6**, 3392 (1994).
[29] D. Swailes and K. Darbyshire, Physica A **242**, 38 (1997).
[30] H. Risken, *The Fokker-Planck Equation* 2nd ed. (Springer-Verlag, Berlin, 1996).
[31] U. Titulaer, Physica A **91**, 321 (1978).
[32] D. Swailes, Y. Sergeev, and A. Parker, Physica A **254**, 517 (1998).
[33] Y. Drossinos, M. Reeks, and D. Swailes (unpublished).